# Heisenberg-limited estimation robust to photon losses in a Mach-Zehnder network with squeezed light

Dario Gatto
*School of Mathematics and Physics, University of Portsmouth, Portsmouth PO1 3QL, United Kingdom*

Paolo Facchi
*Dipartimento di Fisica and MECENAS, Università di Bari, I-70126 Bari, Italy and INFN, Sezione di Bari, I-70126 Bari, Italy*

Vincenzo Tamma*
*School of Mathematics and Physics, University of Portsmouth, Portsmouth PO1 3QL, United Kingdom and Institute of Cosmology and Gravitation, University of Portsmouth, Portsmouth PO1 3FX, United Kingdom*

(Received 30 July 2021; accepted 5 January 2022; published 20 January 2022)

We propose a quantum metrological protocol based on a Mach-Zehnder interferometer with a squeezed vacuum input state and an antisqueezing operation at one of its output channels. A simple and intuitive geometrical picture of the state evolution is provided by the marginal Wigner functions of the state at each interferometer output channel. The protocol allows us to detect the values of the sum $\beta = \frac{1}{2}(\varphi_1 + \varphi_2) + \theta_{\text{in}} - \theta_{\text{out}}$, of the relative phase $\theta_{\text{in}} - \theta_{\text{out}}$ between the two squeezers, and of the average of the phase delays $\varphi_1$ and $\varphi_2$ in the two arms of the interferometer. The detection sensitivity scales at the Heisenberg limit and, remarkably, is robust not only to detector inefficiencies but also to any photon losses occurring before the antisqueezing operation. Interestingly, we demonstrate that in the latter case an increase of sensitivity can even occur by increasing the losses in a suitable range.

DOI: 10.1103/PhysRevA.105.012607

## I. INTRODUCTION

After Caves demonstrated, in a seminal work, that it is possible to reduce the quantum-mechanical noise of the signal in an interferometric experiment by fully harnessing the quantum nature of photons [1], a great deal of interest has been invested in this endeavor, leading to the birth of the field of quantum metrology [2–8]. In the near future, these technologies are expected to find applications in a wide range of settings. For instance, they could enhance the sensitivity in the mapping of inhomogeneous magnetic fields [9–13], phase imaging [14–19], quantum-enhanced nanoscale nuclear magnetic resonance imaging [20–22], and long-distance clock synchronization [23]. Single-parameter quantum metrology, i.e., the problem of estimating a single parameter with quantum measurements, has been extensively studied. By contrast the multiparameter setting has remained vastly unexplored and has only recently become an attractive topic among the quantum physics research community [20,24–32] because of its impact on the development of quantum technologies [33–36].

A simple scenario with multiple unknown parameters is given by a Mach-Zehnder interferometer with two unknown phases in its upper and lower paths. Heisenberg-limited sensitivity to the sum of such phases was shown to be potentially achievable by demonstrating Heisenberg scaling in the quantum Fisher information [31]. However, it is only by demonstrating Heisenberg scaling in the Fisher information associated with specific feasible measurements that one can claim the experimental feasibility of such quantum-enhanced sensitivity [37].

In this work, we consider the Mach-Zehnder interferometer in Fig. 1 where either the phases $\varphi_1$ and $\varphi_2$ in the interferometer paths or the phases associated with the input squeezing operation and the output antisqueezing operation $\theta_{\text{in}}$ and $\theta_{\text{out}}$ are unknown. We aim to answer the following questions. Is it possible to estimate experimentally with Heisenberg-limited sensitivity a combination of such unknown parameters? How is such a sensitivity affected by losses? Are there experimental scenarios where losses can be advantageous?

Interestingly, we show that it is possible to estimate with Heisenberg-limited sensitivity the combination $\beta = \frac{1}{2}(\varphi_1 + \varphi_2) + \theta_{\text{in}} - \theta_{\text{out}}$ of the relative phase $\theta_{\text{in}} - \theta_{\text{out}}$ between two squeezers and the average of the upper phase $\varphi_1$ and the lower phase $\varphi_2$ in the Mach-Zehnder interferometer in Fig. 1. We can thus estimate not only the average phase in the Mach-Zehnder interferometer if the relative phase of the squeezers has a known constant value stabilized through a standard phase locking procedure but also the relative phase of the squeezers if it is the average phase of the Mach-Zehnder interferometer to assume a known constant value in the experiment. The interferometer is also able to estimate the relative phase $\frac{1}{2}(\varphi_1 - \varphi_2)$ between the two arms of the optical

*vincenzo.tamma@port.ac.uk

 

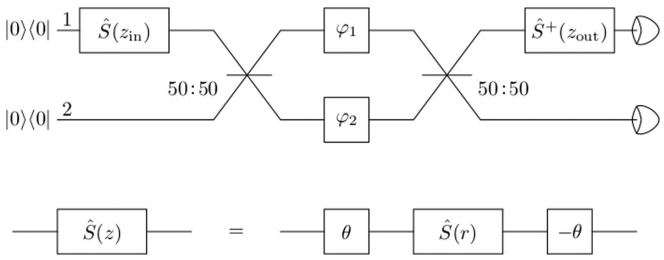


FIG. 1. Interferometric setup for the Heisenberg-limited estimation of the combination $\beta = \frac{1}{2}(\varphi_1 + \varphi_2) + \theta_{\rm in} - \theta_{\rm out}$. Squeezing operations are characterized by the complex squeezing parameter $z = r\,e^{i\theta}$. Specifically, a balanced Mach-Zehnder interferometer is preceded by a squeezer with squeezing parameter $z = z_{\rm in} = re^{i\theta_{\rm in}}$ and followed by an antisqueezing operation with squeezing parameter $z = z_{\rm out} = re^{i\theta_{\rm out}}$. On-off photodetectors are placed at the end of the interferometer.

interferometer with a sensitivity scaling at the standard quantum limit. Remarkably, we demonstrate that in both cases the effect of inefficient detectors only hinders the sensitivity by a constant factor, i.e., that our protocol is robust to external photon losses. This is a particularly desirable feature, as it is the case that other supersensitive schemes employing squeezed states—such as the ones relying on parity measurement—which, in theory, can reach the Heisenberg limit are, in practice, spoiled by the slightest photon loss.

Finally, we compare the effects of detector inefficiencies to losses of photons inside the interferometric circuit, which often have a more severe nature than the former [38,39]. Our work also motivates further analysis of internal losses due to imperfections in the Mach-Zehnder optical elements, which are beyond the scope of the present paper. We show that the Heisenberg-limited scaling not only is also preserved in the presence of losses before the antisqueezing operation but can exhibit, quite counterintuitively, an increase in the sensitivity at a suitable range with high loss values.

## II. STATE EVOLUTION THROUGH THE INTERFEROMETER

Let us consider a balanced Mach-Zehnder interferometer (see the schematic in Fig. 1) in which one of the input channels is fed with a squeezed vacuum state, characterized by the squeezing parameter $z_{\rm in} = re^{i\theta_{\rm in}}$ and the other channel is left in the vacuum state. Throughout the interferometer the system is in a Gaussian state described by the Wigner function [40]

$$W_\sigma(\boldsymbol{\xi}) = \frac{e^{-\frac{1}{2}\boldsymbol{\xi}^T\sigma^{-1}\boldsymbol{\xi}}}{(2\pi)^2\sqrt{\det(\sigma)}}, \tag{1}$$

where $\boldsymbol{\xi} = (x_1, p_1, x_2, p_2)^T$ is the two-mode phase-space variable and $\sigma$ is the covariance matrix.

At the input of the interferometer, the covariance matrix takes the form

$$\sigma_{\rm in} = \frac{1}{2}\begin{pmatrix} S(z_{\rm in})^2 & 0 \\ 0 & \mathbb{1}_2 \end{pmatrix}, \tag{2}$$

where

$$S(z) = S(re^{i\theta}) = e^{i\theta\sigma_y}\,\mathrm{diag}(e^r, e^{-r})\,e^{-i\theta\sigma_y} \tag{3}$$

is the matrix associated with the (one-mode) squeezing operation in phase space acting on the first channel and $\sigma_y$ is the second Pauli matrix. The mean photon number associated with the input state is $\frac{1}{2}\mathrm{tr}(\sigma_{\rm in}) - 1 = \sinh(r)^2 = N$.

The action of the Mach-Zehnder interferometer on the quantum state is described by the covariance matrix transformation

$$\sigma_{\rm MZ} = O_{\rm MZ}\sigma_{\rm in}O_{\rm MZ}^T, \tag{4}$$

where the orthogonal and symplectic matrix $O_{\rm MZ}$ reads [41] (see Appendix A)

$$O_{\rm MZ} = \begin{pmatrix} c_-\,e^{-i\varphi_+\sigma_y} & s_-\,e^{-i(\varphi_+ + \frac{\pi}{2})\sigma_y} \\ s_-\,e^{-i(\varphi_+ + \frac{\pi}{2})\sigma_y} & c_-\,e^{-i\varphi_+\sigma_y} \end{pmatrix}, \tag{5}$$

with $c_- = \cos(\varphi_-)$, $s_- = \sin(\varphi_-)$, and

$$\varphi_\pm = (\varphi_1 \pm \varphi_2)/2. \tag{6}$$

The measurement operation at the output of the Mach-Zehnder interferometer is defined by an antisqueezing operation on the first channel, characterized by the squeezing parameter $z_{\rm out} = re^{i\theta_{\rm out}}$ and by the consequent projection over the vacuum state via on-off photodetectors placed at the two output channels. The operator associated with such a measurement is the projector

$$\hat{\Pi} = \hat{S}_1(z_{\rm out})|00\rangle\langle 00|\hat{S}_1^\dagger(z_{\rm out}), \tag{7}$$

where $\hat{S}_1(z) = e^{\frac{1}{2}(z\hat{a}_1^{\dagger 2} - z^*\hat{a}_1^2)}$ is the squeezing operator and is associated with the Wigner function $W_{\sigma_{\rm out}}(\boldsymbol{\xi})$, with

$$\sigma_{\rm out} = \frac{1}{2}\begin{pmatrix} S(z_{\rm out})^2 & 0 \\ 0 & \mathbb{1}_2 \end{pmatrix} \tag{8}$$

and $S(z_{\rm out})$ given by Eq. (3). The probability for ideal detectors to click is $1 - P$, where

$$\begin{aligned} P = \langle\hat{\Pi}\rangle &= (2\pi)^2\int W_{\sigma_{\rm out}}(\boldsymbol{\xi})\,W_{\sigma_{\rm MZ}}(\boldsymbol{\xi})\,d^4\xi \\ &= \det(\sigma_{\rm MZ} + \sigma_{\rm out})^{-1/2}, \end{aligned} \tag{9}$$

as can be seen by taking a simple Gaussian integral. The expectation value is taken on the Mach-Zehnder output state associated with the covariance matrix $\sigma_{\rm MZ}$ in Eq. (4).

We can track the evolution of the state throughout the interferometer by using the marginals of the correspondent Wigner function,

$$W_i(x_i, p_i; \sigma) = \int W_\sigma(\boldsymbol{\xi})\,dx_j dp_j, \tag{10}$$

at each channel $i, j = 1, 2$ and $i \neq j$, where $W_\sigma$ is given in Eq. (1). Of course, since the state in the two channels gets entangled by the interactions with the beam splitters, the information provided by the marginals cannot be expected to be complete. Nonetheless, as we shall see, the marginals are sufficient to provide a clear and intuitive physical picture.

Initially, the first channel is in a squeezed state, and the second one is in the vacuum state corresponding to the covariance matrix $\sigma = \sigma_{\rm in}$ in Eq. (2): the marginal $W_2$ has a circular Gaussian profile, while the marginal $W_1$ exhibits an elliptic Gaussian profile with one quadrature below the vacuum level and the other one above it, with the squeezing direction being

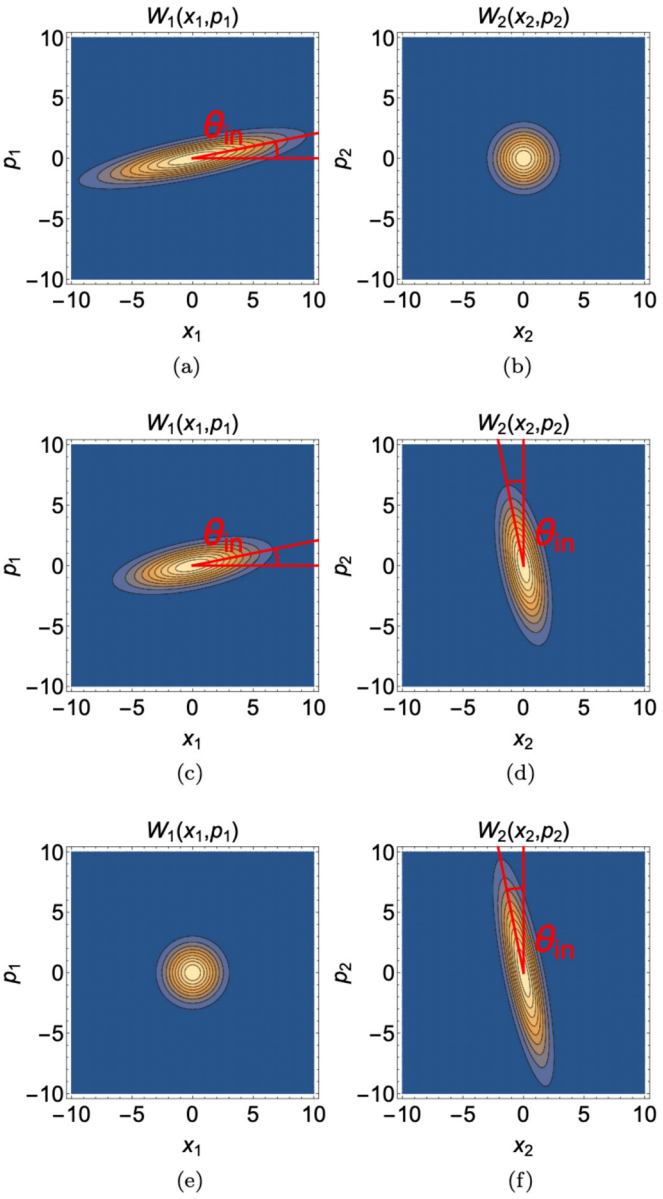


FIG. 2. Contour plots of the marginal Wigner functions defined in Eq. (10) for $\sigma = \sigma_{MZ}$ in Eq. (4) (a) and (b) in the case $\varphi_- = 0$ ($\sigma_{MZ}$ reduces to $\sigma_{in}$ in Eq. (2)), (c) and (d) for $\varphi_- = \pi/4$, and (e) and (f) for $\varphi_- = \pi/2$. The parameter $\varphi_+$ has been set to zero for simplicity. Notice how at the output of the Mach-Zehnder configuration the proportion of photons in each channel, directly related to the squeezing of the ellipses' semiaxes as in Eqs. (11) and (12), shifts from one channel to the other as $\varphi_-$ increases.

determined by the angle $\theta_{in}$ (see Fig. 2 (b) and (a), respectively). After the photons have traversed the Mach-Zehnder configuration, the profiles undergo the measurement described by Eqs. (8) and (9). The parameter $\varphi_-$ controls the squeezing proportions across the two channels and, consequently, also what portion of the photons ends up in which channel (see Fig. 2).

The lengths of the ellipses semiaxes can be found to be

$$1 + \cos(\varphi_-)^2[N \pm \sqrt{N(1+N)}] \tag{11}$$

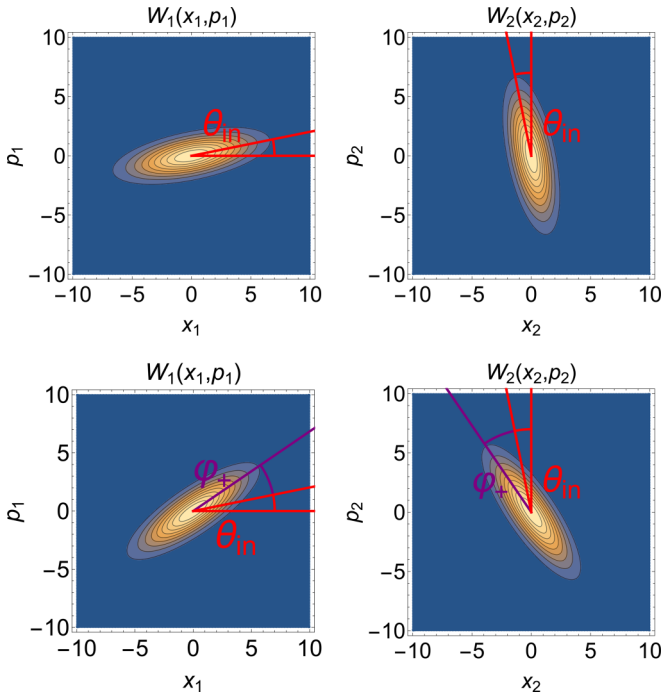


FIG. 3. Comparison between the marginal Wigner functions (10) for $\sigma = \sigma_{MZ}$ in Eq. (4) (a) and (b) in the case where $\varphi_+ = 0$ and (c) and (d) for the ones rotated in phase, corresponding to $\varphi_+ = 0.4$. The parameter $\varphi_-$ has been set to $\pi/4$ for simplicity.

for the first channel and

$$1 + \sin(\varphi_-)^2[N \pm \sqrt{N(1+N)}] \tag{12}$$

for second channel of the interferometer (see Appendix A).

The effect of the parameter $\varphi_+$, often ignored, is to rotate both profiles by an additional angle of $\varphi_+$ in phase space, through the matrix $e^{-i\varphi_+\sigma_y}$ in Eq. (5) (see Fig. 3). As we shall shortly see, $\varphi_+$ has a physical effect on the outcome of the measurement and thus allows us to estimate the average phase of the Mach-Zehnder. Indeed, when the state is antisqueezed with the operation $\hat{S}_1^\dagger(z_{out})$ and then projected onto the vacuum, the detection probability (9) is given by the overlap between the Gaussian Wigner function $W_{\sigma_{MZ}}$ associated with the covariance matrix $\sigma_{MZ}$ in Eq. (4), whose marginals have a total phase $\varphi_+ + \theta_{in}$, and the Gaussian Wigner function $W_{\sigma_{out}}$, whose marginal $W_1$ at the output channel 1 is rotated in phase space by the squeezing angle $\theta_{out}$ associated with the covariance matrix (8). As depicted in Fig. 4, the projection overlap depends on the relative phase

$$\beta = \varphi_+ + \theta_{in} - \theta_{out} \tag{13}$$

between the two Wigner functions, as well as the fraction of photons in the first output channel, and thus on $\varphi_-$. Intuitively, we expect this overlap to be maximal when the ellipse associated with $\sigma_{MZ}$, is squeezed in the same direction as $\sigma_{out}$, i.e., when $\theta_{in} + \varphi_+ = \theta_{out}$.

To account for a detector loss parameter $\eta$ (with $0 < \eta \leqslant 1$), we imagine that the (ideal) detectors are preceded by a fictitious beam splitter with reflectivity $\eta$. This modifies Eq. (9) as

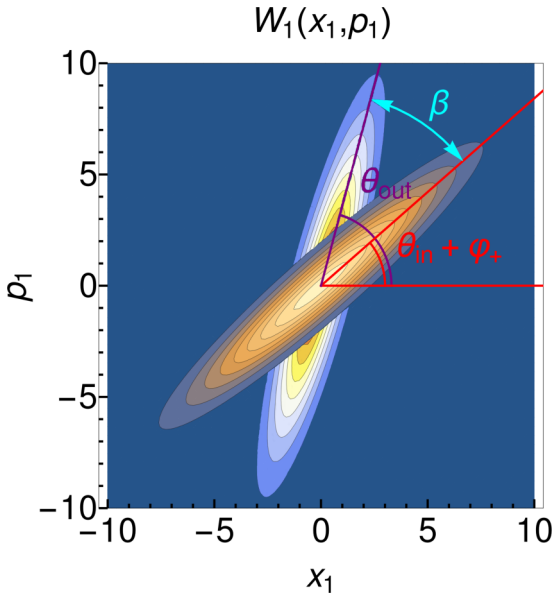


FIG. 4. Marginal Wigner functions associated with the covariance matrices $\sigma_{MZ}$ (foreground) and $\sigma_{out}$ (background), defined in Eqs. (4) and (8), respectively. The relative angle is $\beta = \varphi_+ + \theta_{in} - \theta_{out}$.

follows:

$$P = \det[\eta\,\sigma_{MZ} + (2-\eta)\sigma_{out}]^{-1/2}, \tag{14}$$

as shown in Appendixes B and C. Using expressions (4) and (8) for the covariance matrices, the detection probability (14) reads

$$P(\beta,\varphi_-) = (1+\tilde{\eta}\{2N + [2\cos(\varphi_-)^2 + \tilde{\eta}\sin(\varphi_-)^4]N^2 - 2\cos(\varphi_-)^2\cos(2\beta)N(1+N)\})^{-1/2}, \tag{15}$$

with $\tilde{\eta} = \eta(2-\eta)$ and the relative phase $\beta$ given in Eq. (13). Plots of $P$ as a function of $\beta$ and $\varphi_-$ are provided in Fig. 5 for different values of the mean photon number $N$ and the detector loss parameter $\eta$.

From Eq. (15) and Fig. 5 the periodicity of $P$ with period $\pi$ in both variables is evident; hence, we may restrict our attention to a fundamental domain, such as $|\beta| \leqslant \pi/2$, $|\varphi_-| \leqslant \pi/2$. The detection probability $P$ is maximal for $(\beta,\varphi_-) = (h,k)\,\pi$, with integers $h$ and $k$. As can be seen from Fig. 5, these peaks become more and more localized as $N$ increases, with a variation on the $\beta$ axis significantly more stark than on the $\varphi_-$ axis. A nonunit loss parameter instead spreads out these peaks, an effect which is quickly compensated by a moderate increase of $N$ by a factor which later we will show to be equal to $\sqrt{\tilde{\eta}}$. Furthermore, notice how both $\varphi_-$ and $\beta$ affect the detection probability: the relative angle $\beta$ between the squeezed ellipses [corresponding to $W_{\sigma_{MZ}}$ and $W_{\sigma_{out}}$ in Eq. (9)] has a major physical effect, allowing both the global phase of the Mach-Zehnder $\varphi_+$ and the relative phase of the squeezers $\theta_{in} - \theta_{out}$ to be estimated once the other one is known. Thus, assuming that only the relative phase in a Mach-Zehnder interferometer bears physical significance is not correct in general; for a discussion of the cases when this is actually correct see Ref. [37]. In fact, we will see it is impossible to estimate $\beta$ (and hence $\varphi_+$) without any

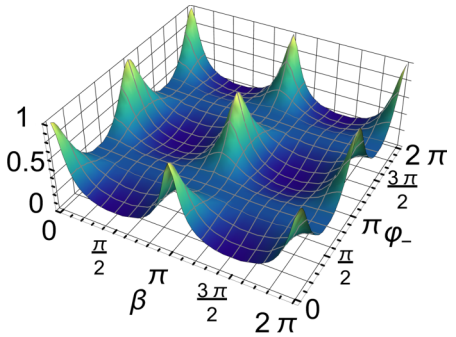


(a) $N = 4$, $\eta = 1$.

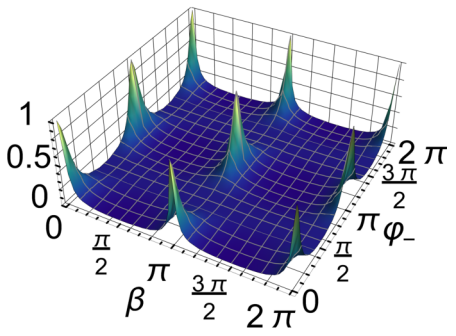


(b) $N = 20$, $\eta = 1$.

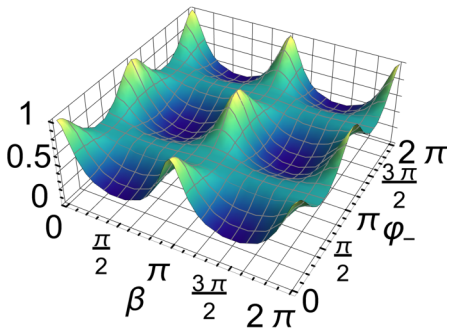


(c) $N = 4$, $\eta = 0.2$.

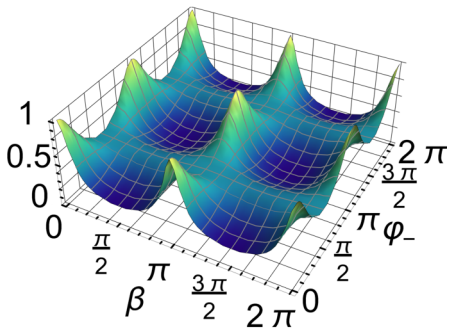


(d) $N = 6.667$, $\eta = 0.2$.

FIG. 5. Detection probability (15) as a function of $\beta = \frac{1}{2}(\varphi_1 + \varphi_2) + \theta_{in} - \theta_{out}$ and $\varphi_- = \frac{1}{2}(\varphi_1 - \varphi_2)$ for (a) $N = 4$, $\eta = 1$, (b) $N = 20$, $\eta = 1$, (c) $N = 4$, $\eta = 0.2$, and (d) $N = 6.667$, $\eta = 0.2$. The maxima of $P$ become more and more localized with the increasing of $N$ and concentrate way more quickly in the $\beta$ direction than they do in the $\varphi_-$ direction. The spread caused by a nonunit loss parameter is compensated by dividing $N$ by the factor $\sqrt{\tilde{\eta}} = \sqrt{\eta(2-\eta)}$, as is evident when comparing the (a) and (d) in the case of $\eta = 0.2$.

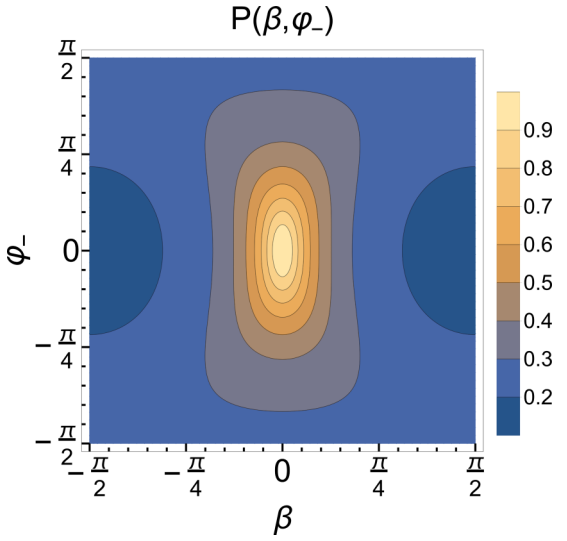


FIG. 6. Level curves for the detection probability $P$ given in Eq. (15). Every couple of parameters corresponding to a point on a given level curve is completely indistinguishable from every other point on the same curve.

knowledge of $\varphi_-$ and vice versa. Of course, in practice, any laser source must be phase locked with respect to a reference phase. This is reflected in the dependence of $P$ on the relative phase *of the squeezers*, $\theta_{\text{in}} - \theta_{\text{out}}$, which shifts the probability plot on the $\beta$ axis. Analogously, one could estimate $\theta_{\text{in}} - \theta_{\text{out}}$ when the known reference phase is the average phase $\varphi_+$ in the network.

## III. ESTIMATION PROCEDURE

Let us now discuss the sensitivity achievable with this estimation scheme. The relative angle of the squeezers—or any other combination of $\varphi_1$, $\varphi_2$, $\theta_{\text{in}}$, and $\theta_{\text{out}}$ over which the experimentalist has good control—can be used to calibrate the estimation apparatus so that the detectors click at almost every trial within the desired confidence level.

The quantum observable measured at the output of the interferometer is the projector $\hat{\Pi}$ in (7), and the detection

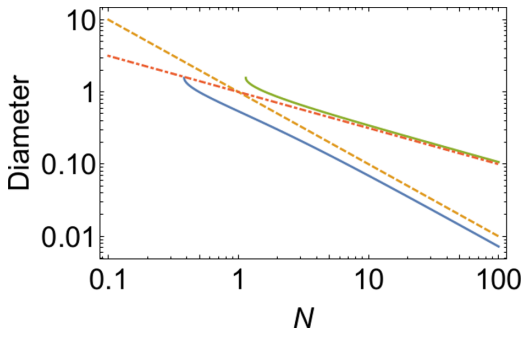


FIG. 7. Diameters for the 90% level curve of the detection probability $P$ as a function of $N$ at $\eta = 1$. The diameter in the $\beta$ direction (bottom solid blue line) is compared with $1/N$ (dashed yellow line), whereas the diameter in the $\varphi_-$ direction (top solid green line) is compared with $1/\sqrt{N}$ (dot-dashed red line).

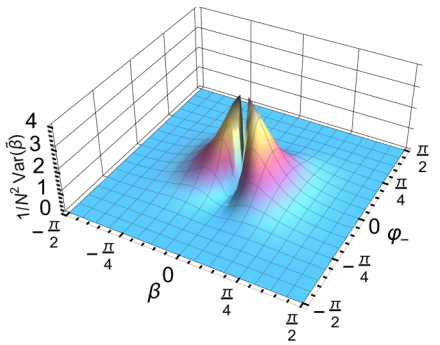

(a) $1/N^2\text{Var}(\widetilde{\beta})$, $N = 2$.

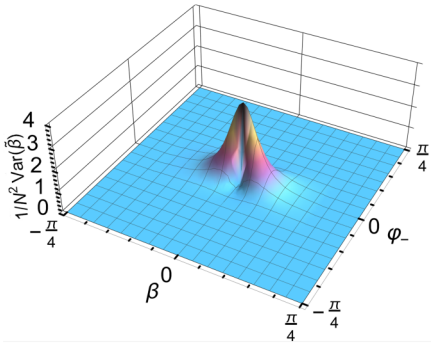

(b) $1/N^2\text{Var}(\widetilde{\beta})$, $N = 20$.

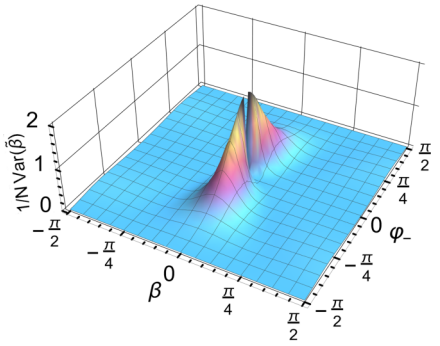

(c) $1/N\text{Var}(\widetilde{\varphi}_-)$, $N = 2$.

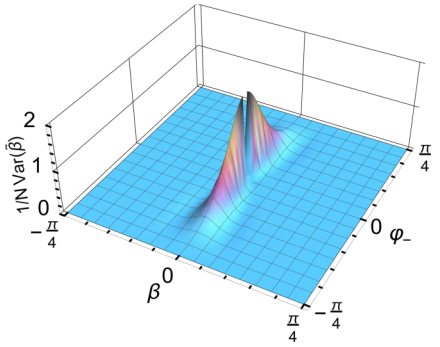

(d) $1/N\text{Var}(\widetilde{\varphi}_-)$, $N = 20$.

FIG. 8. Plots of the rescaled inverse variances of $\widetilde{\beta}$ and $\widetilde{\varphi}_-$ for (a) and (c) $N = 2$ and (b) and (d) $N = 20$. If the variance of $\widetilde{\beta}$ is rescaled by $N^2$ and the variance of $\widetilde{\varphi}_-$ is rescaled by $N$, there is a neighborhood of the origin where they both stay constant. The jump discontinuity at the origin is a consequence of the local indistinguishability of the parameters.

probability is given in Eq. (9). In order to correctly estimate $\beta$ or $\varphi_-$ we have to deal with the local indistinguishability of the parameters [42–45]. This means that for any fixed probability $P_0$, a given couple of parameters $(\beta, \varphi_-)$ is indistinguishable from every other point on the curve $P(\beta, \varphi_-) = P_0$, as all possible outcomes of the measurement of $\hat{\Pi}$ have the same probabilities in either case (see Fig. 6). The ambiguity in $\beta$ is removed once the value of $\varphi_-$ is known, but clearly, in practice, $\varphi_-$ cannot be known with arbitrary precision. In the previous section we observed that the peaks concentrate more quickly in the $\beta$ direction than in the $\varphi_-$ direction: more precisely, the horizontal diameter of the level curve corresponding to a fixed probability $P_0$ can be determined directly from Eq. (15) and reads (see Appendix E for details)

$$\beta_* = \arcsin\sqrt{\frac{1-P_0^2}{4\tilde{\eta}N(1+N)P_0^2}}. \tag{16}$$

Similarly, the vertical diameter can be found to be

$$\varphi_* = \arcsin\sqrt{\frac{\sqrt{P_0^2+\tilde{\eta}\left(1-P_0^2\right)}-P_0}{\tilde{\eta}NP_0}}. \tag{17}$$

From these expressions, plotted in Fig. 7 versus $N$, it is evident that the horizontal diameter $\beta_*$ scales as $1/N$, whereas the vertical diameter $\varphi_*$ scales as $1/\sqrt{N}$.

Thus, knowledge of $\varphi_-$ with classical precision will be sufficient to estimate $\beta$ with Heisenberg-limited sensitivity, as the uncertainty in $\varphi_-$ becomes irrelevant for large $N$.

It remains to be shown that the Heisenberg limit can be achieved in this way. If the measurement of $\hat{\Pi}$ in (7) is repeated $n$ times and the outcomes are $x_1, \ldots, x_n$, with $x_i = 0$ or 1 according to whether the detector clicked or not, the maximum likelihood estimator (MLE) $\widetilde{\beta}$ is defined implicitly by the equation

$$P(\widetilde{\beta}, \varphi_-) = \frac{1}{n}\sum_{i=1}^{n} x_i. \tag{18}$$

For large $n$, the variance of $\widetilde{\beta}$ can be approximated as

$$\mathrm{Var}[\widetilde{\beta}] \simeq \frac{\langle\hat{\Pi}^2\rangle - \langle\hat{\Pi}\rangle^2}{n(\partial\langle\hat{\Pi}\rangle/\partial\beta)^2} = \frac{P(\beta,\varphi_-)[1-P(\beta,\varphi_-)]}{n(\partial P/\partial\beta)^2}. \tag{19}$$

When all the terms in expression (19) are nonzero, since from (15) $P \propto 1/N$, one would have that (19) scales as $\mathrm{Var}[\widetilde{\beta}] \propto N$. Thus, we cannot expect a good metrological scaling for generic values of $\beta$ and $\varphi_-$. However in the correspondence of any of the maxima in Fig. 5 we have $P = 1$ independently of $N$, and both the numerator and the denominator of Eq. (19) vanish; we will momentarily show that there is Heisenberg scaling in this case.

A plot of the rescaled sensitivity $1/N^2\mathrm{Var}[\widetilde{\beta}]$, which we report in Fig. 8, shows that there is, in fact, a neighborhood of the origin which stays essentially constant as $N$ increases, indicating there is, indeed, Heisenberg scaling in this region. Interestingly, this suggests constructive quantum interference is a necessary metrological resource to reach the Heisenberg limit. The jump discontinuity at the origin is again a consequence of the local indistinguishability of the parameters: performing the estimation once $\varphi_-$ is known corresponds to taking a *section* of Fig. 8 at fixed $\varphi_-$, and each of these sections is well defined and free from singularities.

Therefore, we require $\varphi_- \simeq h\pi$, where $h$ is an integer, with classical precision. Besides making sure the sensitivity (19) stays close to its maximal value, where Heisenberg scaling is expected, the condition $\varphi_- \simeq h\pi$ entails that all photons end up in the first channel, offering the practical advantage of having to place only one detector at the output of the interferometer.

Moreover, our discussion indicates the size of the Heisenberg-limited region about a maximum scales as $1/N$ in the $\beta$ direction. Taking these facts into account, we can expand expression (19) around its maxima, that is, $\beta = k\pi + \delta\beta$ and $\varphi_- = h\pi + \delta\varphi$, with $|\delta\beta| \leqslant \beta_*$ and $|\delta\varphi| \leqslant \varphi_*$, and obtain

$$\begin{aligned}\mathrm{Var}[\widetilde{\beta}] &= \left.\frac{P(\beta,\varphi_-)[1-P(\beta,\varphi_-)]}{n(\partial P/\partial\beta)^2}\right|_{\beta=k\pi+\delta\beta,\varphi_-=h\pi+\delta\varphi} \\ &= \frac{1}{32\tilde{\eta}nN^2} + \frac{[1+\tilde{\eta}(2\delta\beta^2N^2+\delta\varphi^2N)](\sqrt{1+\tilde{\eta}\delta\beta^2N^2}-1)(2\delta\beta^2N^2+\delta\varphi^2N)}{24\tilde{\eta}^2\delta\beta^2nN^5} + O\left(\frac{1}{N^4}\right).\end{aligned} \tag{20}$$

Since $\delta\beta = O(1/N)$ and $\delta\varphi = O(1/\sqrt{N})$, the first term in Eq. (20), which scales as $1/N^2$, is the dominant one, with the second term being of order $1/N^3$. Hence, the estimation of $\beta$ can be achieved at the Heisenberg limit, with the statistical error

$$\mathrm{Var}[\widetilde{\beta}] = \frac{1}{32\eta(2-\eta)nN^2}, \tag{21}$$

with only classical *a priori* knowledge of $\varphi_-$ around a peak of maximal probability.

Such Heisenberg scaling is obviously consistent, apart from a constant factor, with the quantum Cramér-Rao bound for the estimation of $\varphi_+$ found in Ref. [31] for a fixed value of $\theta_{\mathrm{in}}$. We remark that in the presence of inefficient detectors, corresponding to $\eta < 1$, the variance of the estimator (21) changes only by a constant factor $1/[\eta(2-\eta)]$ with respect to the ideal case ($\eta = 1$), meaning that the effect of such losses does not affect the Heisenberg scaling and is easily mitigated by increasing the mean photon number by the square root of the same constant factor (see again Fig. 5).

It is possible to reverse the roles of the parameters; that is, once $\beta$ is known with classical precision, we can use the same procedure to estimate $\varphi_-$. To this end, given the measurements $x_1, \ldots, x_n$, the maximum likelihood estimator $\widetilde{\varphi}_-$ is now defined by

$$P(\beta, \widetilde{\varphi}_-) = \frac{1}{n}\sum_{i=1}^{n} x_i. \tag{22}$$

Similar to Eq. (19), for large $n$ the variance of $\widetilde{\varphi}_-$ can be approximated by the error-propagation formula

$$\mathrm{Var}[\widetilde{\varphi}_-] \simeq \frac{P(\beta,\varphi_-)[1-P(\beta,\varphi_-)]}{n(\partial P/\partial\varphi_-)^2}. \tag{23}$$

A plot of $1/N\mathrm{Var}[\widetilde{\varphi}_-]$ in Fig. 8 reveals that much like the case of $\beta$, there is a neighborhood of the origin where the sensitivity is maximal, although the scaling with $N$ is classical. Indeed, setting $\beta \simeq k\pi$, where $k$ is and integer, with classical precision and assuming $\varphi_-$ to be in a neighborhood of $h\pi$ of size $1/N$, we have

$$\begin{aligned}\mathrm{Var}[\widetilde{\varphi}_-] &\simeq \left.\frac{P(\beta,\varphi_-)[1-P(\beta,\varphi_-)]}{n(\partial P/\partial\varphi_-)^2}\right|_{\beta=k\pi+\delta\beta,\,\varphi_-=h\pi+\delta\varphi} \\ &= \frac{1}{4\tilde{\eta}nN} + \frac{6[\tilde{\eta}N(2\delta\varphi^2N+\delta\beta^2)+(5-\tilde{\eta})\delta\beta^2]}{24\tilde{\eta}nN^2} \\ &\quad + O\left(\frac{1}{N^3}\right),\end{aligned} \tag{24}$$

with $\delta\beta = O(1/\sqrt{N})$ and $\delta\varphi = O(1/N)$. The second term is $O(1/N^2)$ hence the dominant term is the first one and does not depend on $\delta\beta$ or $\delta\varphi$. Therefore, our protocol enables the estimation of $\varphi_-$ as well, with sensitivity scaling at the standard quantum limit.

A final remark is in order. There are other situations in which we are able to reach the Heisenberg limit in the estimation of $\beta$. If $\varphi_-$ is not a multiple of $\pi$, but rather $\varphi_- = (k+\frac{1}{2})\pi$ with integer $k$, all the photons end up in the second channel rather than the first. This suggests that in this case it might be possible to obtain the same results as above simply by performing the antisqueezing operation on the second channel instead of the first one. Indeed, in this case the detection probability becomes

$$\begin{aligned}P'(\beta,\varphi_-) = (1+\tilde{\eta}\{2N+[2\sin(\varphi_-)^2+\tilde{\eta}\cos(\varphi_-)^4]N^2 \\ -2\sin(\varphi_-)^2\cos(2\beta)N(1+N)\})^{-1/2}.\end{aligned} \tag{25}$$

We can clearly see that $P'(\beta,\varphi_- - \pi/2) = P(\beta,\varphi_-)$; hence, as expected, we can repeat the procedures outlined before for the estimation of both $\beta$ and $\varphi_-$, with the only difference being that the peaks of $P$ in $(\beta,\varphi_-) = (h,k)\pi$ are now replaced by $(h, k+\frac{1}{2})\pi$, but otherwise, with identical results.

## IV. INTERNAL LOSSES

We now compare the effect of *internal losses*, i.e., losses of photons which happen inside the interferometric circuit, to *external losses*, i.e., the previous kind of losses due to detector inefficiencies. Typically, it is found that the former have a tendency to be more disruptive than the latter [38].

We can implement internal losses by means of a fictitious beam splitter with reflectivity $\eta$ placed *before* the antisqueezer. In this configuration, the detection probability now reads (see Appendix C)

$$P'' = \det\left(\eta\,\sigma_{\mathrm{MZ}} + \frac{1-\eta}{2}\,\mathbb{I}_4 + \sigma_{\mathrm{out}}\right)^{-1/2}. \tag{26}$$

Using expressions (4), (5), and (2) for the covariance matrices, the expression above becomes

$$\begin{aligned}P''(\beta,\varphi_-) = \{1+[1+\eta(2-\eta)]N \\ +\eta[2-\eta+\eta\cos(\varphi_-)^4]N^2 \\ -2\cos(\varphi_-)^2\cos(2\beta)N(1+N)\}^{-1/2}.\end{aligned} \tag{27}$$

We now use this new probability to reconstruct the MLE $\widetilde{\beta}$. Substituting $P''$ in Eq. (19) and following the procedure outlined in the previous section (about the origin, for simplicity), we find

$$\begin{aligned}\mathrm{Var}[\widetilde{\beta}] \simeq \frac{\sqrt{1-\eta}(9+21\eta-224\eta^2+65\eta^3+945\eta^4)+(1+\eta^2)(2-4\eta+21\eta^2-38\eta^3+38\eta^4)}{1208\eta^2(1+\eta)^3N^2} \\ +\frac{B_3}{234\eta^2(1+\eta)\delta\beta^2N^4}+O\left(\frac{1}{N^4}\right),\end{aligned} \tag{28}$$

where $\delta\beta = O(1/N)$, $\delta\varphi = O(1/\sqrt{N})$, and

$$\begin{aligned}B_3 = 2\eta(2-\sqrt{1-\eta})[37\sqrt{1-\eta}-(12-\eta)(3\eta-29)+81\delta\beta^2N^2]\sqrt{3\eta-\eta^2(1-\delta\varphi^2N-\delta\beta^2N^2)} \\ +\eta[59+(\eta+97)\sqrt{1-\eta}+30\eta(17\eta+3\delta\varphi^2N)-88(2+\eta^2)\delta\beta^2N^2]\sqrt{5\eta^2-4\eta^3+\delta\beta^2N^2}.\end{aligned} \tag{29}$$

The analogous expression for the MLE $\widetilde{\varphi}_-$ is

$$\begin{aligned}\mathrm{Var}[\widetilde{\varphi}_-] = \frac{45\sqrt{1-\eta}+11[13-2\eta+11\eta^2(1+\eta)(5-\eta)]+7\eta^3[40\sqrt{1-\eta}+61\eta^2(24+85\sqrt{1-\eta})-4\eta(12+75\sqrt{1-\eta})]}{680\eta(1+\eta)^6N} \\ +\frac{F_2}{103\eta^5(1+\eta)^7\delta\varphi^2N^4}+O\left(\frac{1}{N^3}\right),\end{aligned} \tag{30}$$

where now $\delta\beta = O(1/\sqrt{N})$, $\delta\varphi = O(1/N)$, and

$$\begin{aligned}F_2 = 64\eta[90+\delta\varphi^2N^2+\delta\beta^2N-28\sqrt{1-\eta}+20\eta(303\sqrt{1-\eta}-64)] \\ +64\eta^2[10+\delta\varphi^2N^2+265\sqrt{2-\delta\varphi^2N^2-\eta}+10\eta(128+7\sqrt{1-\eta})]+7\eta(1-\eta).\end{aligned} \tag{31}$$

These terms are plotted in Fig. 9. In Fig. 9(a) we can see that, comparing the leading term of Eq. (20) to the leading term of Eq. (28), the sensitivity of $\widetilde{\beta}$ still scales at the Heisenberg limit in the presence of internal losses (again, modulo constant factors), but for a noise level between roughly 0.25 and 0.45 our protocol performs *better* under internal losses. This type of phenomenon, which may at first glance appear rather surprising, is actually not uncommon in the quantum estimation literature, where it is known as *dithering* [46]. What is more interesting is the fact that dithering can, in fact, occur in the presence of a nonunitary disturbance.

In Fig. 9(c) we can see that the same phenomenon occurs for $\widetilde{\varphi}_-$: comparing the leading term of Eq. (24) with the leading term of Eq. (29), we observe that for $\eta$ approximately between 0.15 and 0.47 the protocol performs better under internal losses than it does under external losses (although the scaling does not surpass the standard quantum limit). The next-to-leading terms, on the other hand, are always larger in the case of internal losses than they are in the case of external losses, but of course, they become irrelevant in the limit of large $N$.

## V. DISCUSSION

We have provided a quantum metrological protocol which makes use of squeezing operations, on-off detectors, and quantum interference as metrological resources to achieve the Heisenberg limit in the estimation of either the average phase in a Mach-Zehnder interferometer or the relative phase of the two given squeezers. The protocol also allows us to estimate the relative phase between the two arms of the Mach-Zehnder network at the standard quantum limit.

Our protocol shows not only that the "global phase" in a Mach-Zehnder interferometer has a physical effect, which allows it to be detected, but also that in general its knowledge is necessary even if one wishes to estimate other parameters. Indeed, while we choose to focus primarily on the estimation of $\beta$, the local indistinguishability of $(\beta, \varphi_-)$ entails that any attempt at estimating $\varphi_-$ cannot be carried out without some knowledge of the value $\beta$ independent of one's expectations for the sensitivity of the estimation procedure. This might come in the form of knowledge of the parameter, as we have done, or, for instance, in the form of a reasonably justified prior distribution, which would transform the protocol into a Bayesian estimation problem [42,44]. Remarkably, despite the local indistinguishability of the parameters, it is possible to determine $\beta$ with Heisenberg precision with only a classical knowledge of $\varphi_-$.

The physical effect of the parameters $\beta$ of $\varphi_-$ is most easily understood in the phase-space picture. The parameter $\beta$ represents the relative angle between the ellipse associated with the state after the Mach-Zehnder configuration and the ellipse associated with the output of the interferometer right before detection. On the other hand, $\varphi_-$ controls the squeezing ratio between the first and second channels of the interferometer. Both these effects contribute to the interference pattern observed in the detection probability $P$ as a function of $\beta$ and $\varphi_-$. The role of constructive quantum interference as a necessary condition for achieving the Heisenberg limit in distributed quantum metrology is a particularly interesting element which

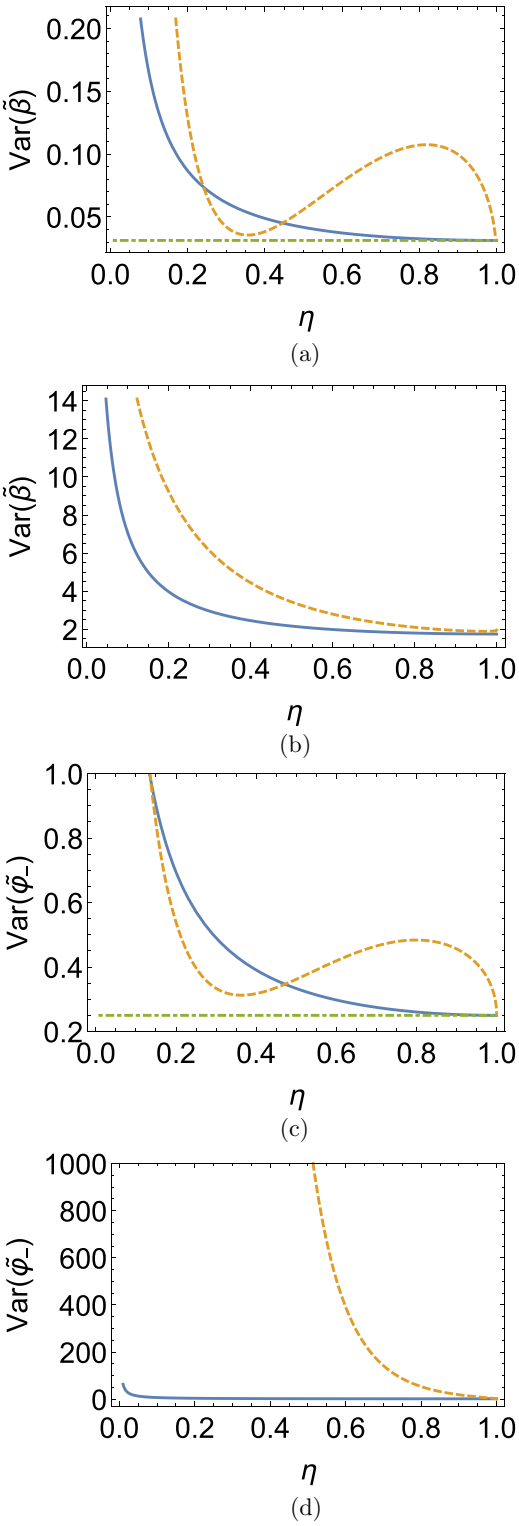


FIG. 9. Comparison of (a) and (c) the leading terms and (b) and (d) next-to-leading terms for the MLEs $\widetilde{\beta}$ and $\widetilde{\varphi}_-$ as a function of the loss parameter $\eta$ under external losses (blue solid lines) and under internal losses (yellow dashed lines). For a noise level roughly between 50% and 70% internal losses provide an advantage. The noiseless values ($\eta = 1$, green dot-dashed lines) are also depicted for reference.

emerges from our analysis and will be further explored in future works.

Remarkably, we have shown that the protocol is robust to detector inefficiency, which in practice could seriously hinder the estimation sensitivity with respect to the ideal case but actually only reduces the sensitivity by a constant factor and can thus be overcome by increasing the mean photon number by the same amount. Moreover, internal photon losses, which tend to hinder metrological sensitivity more dramatically than external ones, turn out to also just reduce the sensitivity by a constant factor, and when the losses are relatively high (roughly between 50% and 70%), a further increase in internal losses leads to an enhancement of the signal due to an unexpected dithering effect. Finally, this work also established the basis for future studies of the impact on quantum estimation of dark noise in the detectors.

## ACKNOWLEDGMENTS

This work was partially supported by the Office of Naval Research (ONR) Global (Award No. N62909-18-1-2153). D.G. is supported by the University of Portsmouth. P.F. is partially supported by Istituto Nazionale di Fisica Nucleare (INFN) through the project "QUANTUM" and by the Italian National Group of Mathematical Physics of Istituto Nazionale di Alta Matematica (GNFM-INdAM).

## APPENDIX A: SQUEEZING OF THE STATE AT THE TWO OUTPUT CHANNELS OF THE MACH-ZEHNDER NETWORK

The lengths of the semiaxes of the ellipses describing the marginal Wigner functions in Eq. (10) at channels 1 and 2 of the Mach-Zehnder network as shown in Figs. 2 and 3 can be calculated by expressing the covariance matrix $\sigma = \sigma_{\rm MZ}$ in Eq. (4) in block form as

$$\sigma_{\rm MZ} = \begin{pmatrix} \sigma_1 & \tau \\ \tau^T & \sigma_2 \end{pmatrix}, \tag{A1}$$

where

$$\sigma_1 = \begin{pmatrix} s_+^{(1)} & \cos(\varphi_+)\sin(2\varphi_+ + 2\theta_{\rm in})^2\sqrt{N(1+N)} \\ \cos(\varphi_+)\sin(2\varphi_+ + 2\theta_{\rm in})^2\sqrt{N(1+N)} & s_-^{(1)} \end{pmatrix},$$
$$\sigma_2 = \begin{pmatrix} s_-^{(2)} & -\sin(\varphi_-)^2\sin(2\varphi_+ + 2\theta_{\rm in})\sqrt{N(1+N)} \\ \sin(\varphi_-)^2\sin(2\varphi_+ + 2\theta_{\rm in})\sqrt{N(1+N)} & s_+^{(2)} \end{pmatrix},$$
$$\tau = \frac{1}{2}\begin{pmatrix} -\sin(2\varphi_-)\sin(2\varphi_+ + 2\theta_{\rm in})\sqrt{N(1+N)} & \tau_-, \\ \tau_+\sin(2\varphi_-)\sin(2\varphi_+ + 2\theta_{\rm in})\sqrt{N(1+N)} & \end{pmatrix},$$

and

$$s_\pm^{(1)} = \tfrac{1}{2}\{1 + 2\cos(\varphi_-)^2\sqrt{N}[\sqrt{N} \pm \cos(2\varphi_+ + 2\theta_{\rm in})\sqrt{1+N})]\},$$
$$s_\pm^{(2)} = \tfrac{1}{2}\{1 + 2\sin(\varphi_-)^2\sqrt{N}[\sqrt{N} \pm 2\cos(2\varphi_+ + \theta_{\rm in})\sqrt{1+N})]\},$$
$$\tau_\pm = \sin(2\varphi_-)\sqrt{N}[\cos(2\varphi_+ + 2\theta_{\rm in})\sqrt{1+N} \pm \sqrt{N}]. \tag{A2}$$

The lengths of the two semiaxes of the marginal Wigner function $W_1(x_1, p_1; \sigma_{\rm MZ})$ at the first channel are given by the eigenvalues of $\sigma_1$ and read

$$1 + \cos(\varphi_-)^2[N \pm \sqrt{N(1+N)}], \tag{A3}$$

as reported in Eq. (11) in the main text, whereas the lengths of the two semiaxes of the marginal Wigner function $W_2(x_2, p_2; \sigma_{\rm MZ})$ at the second channel are given by the eigenvalues of $\sigma_2$,

$$1 + \sin(\varphi_-)^2[N \pm \sqrt{N(1+N)}], \tag{A4}$$

which in turn give Eq. (12).

## APPENDIX B: LINEAR OPTICAL NETWORKS IN PHASE SPACE

A passive linear optical network is described by a unitary operator $\hat{U}$ on the underlying Hilbert space of the two-mode electromagnetic field, which acts on the annihilation operators according to the relation

$$\hat{U}^\dagger \hat{a}_i \hat{U} = \sum_{j=1}^{2} \mathcal{U}_{ij}\,\hat{a}_j, \tag{B1}$$

where $\mathcal{U}$ is a $2 \times 2$ unitary matrix.

Consider the vector of the quadratures $\hat{\mathbf{R}} = (\hat{x}_1, \hat{p}_1, \hat{x}_2, \hat{p}_2)^T$, with $\hat{x}_j = (\hat{a}_j + \hat{a}_j^\dagger)/\sqrt{2}$ and $\hat{p}_j = (\hat{a}_j - \hat{a}_j^\dagger)/\sqrt{2}i$. By defining the unitary $4 \times 4$ matrix

$$W = \frac{1}{\sqrt{2}} \bigoplus_{j=1}^{2} \begin{pmatrix} 1 & i \\ 1 & -i \end{pmatrix}, \tag{B2}$$

we have the identity

$$\hat{\mathbf{A}} := (\hat{a}_1, \hat{a}_1^\dagger, \hat{a}_2, \hat{a}_2^\dagger)^T = W\hat{\mathbf{R}}. \tag{B3}$$

Thus, the network transforms the quadratures according to

$$\begin{aligned} \hat{U}^\dagger \hat{R}_i \hat{U} &= \hat{U}^\dagger \sum_{j=1}^{2} (W_{i,2j-1}^\dagger \hat{a}_j + W_{i,2j}^\dagger \hat{a}_j^\dagger)\hat{U} = \sum_{j,k=1}^{2} (W_{i,2j-1}^\dagger \mathcal{U}_{jk} \hat{a}_k + W_{i,2j}^\dagger \mathcal{U}_{jk}^* \hat{a}_k^\dagger) \\ &= \sum_{h=1}^{4} \sum_{j,k=1}^{2} (W_{i,2j-1}^\dagger \mathcal{U}_{jk} W_{2k-1,h} + W_{i,2j}^\dagger \mathcal{U}_{jk}^* W_{2k,h})\hat{R}_h := \sum_{h=1}^{4} O_{ih} \hat{R}_h, \end{aligned} \tag{B4}$$

that is,

$$\hat{U}^\dagger \hat{\mathbf{R}} \hat{U} = O\hat{\mathbf{R}}. \tag{B5}$$

The matrix $O$ has the form

$$O = W^\dagger \begin{pmatrix} \mathcal{U}_{11} & 0 & \mathcal{U}_{12} & 0 \\ 0 & \mathcal{U}_{11}^* & 0 & \mathcal{U}_{12}^* \\ \mathcal{U}_{21} & 0 & \mathcal{U}_{22} & 0 \\ 0 & \mathcal{U}_{21}^* & 0 & \mathcal{U}_{22}^* \end{pmatrix} W, \tag{B6}$$

which, as can be easily verified, is both orthogonal and symplectic and can be simplified as follows:

$$O = \begin{pmatrix} \mathrm{Re}(\mathcal{U}_{11})\mathbb{1}_2 - i\,\mathrm{Im}(\mathcal{U}_{11})\sigma_y & \mathrm{Re}(\mathcal{U}_{12})\mathbb{1}_2 - i\,\mathrm{Im}(\mathcal{U}_{12})\sigma_y \\ \mathrm{Re}(\mathcal{U}_{21})\mathbb{1}_2 - i\,\mathrm{Im}(\mathcal{U}_{21})\sigma_y & \mathrm{Re}(\mathcal{U}_{22})\mathbb{1}_2 - i\,\mathrm{Im}(\mathcal{U}_{22})\sigma_y \end{pmatrix}. \tag{B7}$$

The two-mode covariance matrix is defined as $\sigma = (\sigma_{jk})$, where

$$\sigma_{jk} = \tfrac{1}{2}\langle\{\hat{R}_j, \hat{R}_k\}\rangle - \langle\hat{R}_j\rangle\langle\hat{R}_k\rangle, \tag{B8}$$

with the expectation value taken on the field state. Therefore, if the field has initial covariance $\sigma_{\mathrm{in}}$, after the action of a passive linear optical network it has a covariance given by

$$\sigma_{\mathrm{out}} = O\sigma_{\mathrm{in}}\, O^T, \tag{B9}$$

which is nothing but a (symplectic) rotation in phase space.

In the case of the Mach-Zehnder interferometer, the unitary matrix $\mathcal{U}$ matrix reads

$$\mathcal{U}_{\mathrm{MZ}} = \frac{1}{2}\begin{pmatrix} 1 & -i \\ -i & 1 \end{pmatrix}\begin{pmatrix} e^{i\varphi_1} & 0 \\ 0 & e^{i\varphi_2} \end{pmatrix}\begin{pmatrix} 1 & i \\ i & 1 \end{pmatrix} = e^{i\varphi_+}\begin{pmatrix} \cos(\varphi_-) & -\sin(\varphi_-) \\ \sin(\varphi_-) & \cos(\varphi_-) \end{pmatrix}; \tag{B10}$$

hence, the corresponding rotation in phase space is given by

$$O_{\mathrm{MZ}} = \begin{pmatrix} \cos(\varphi_+)\cos(\varphi_-) & -\sin(\varphi_+)\cos(\varphi_-) & -\cos(\varphi_+)\sin(\varphi_-) & \sin(\varphi_+)\sin(\varphi_-) \\ \sin(\varphi_+)\cos(\varphi_-) & \cos(\varphi_+)\cos(\varphi_-) & -\sin(\varphi_+)\sin(\varphi_-) & -\cos(\varphi_+)\sin(\varphi_-) \\ \cos(\varphi_+)\sin(\varphi_-) & -\sin(\varphi_+)\sin(\varphi_-) & \cos(\varphi_+)\cos(\varphi_-) & -\sin(\varphi_+)\cos(\varphi_-) \\ \sin(\varphi_+)\sin(\varphi_-) & \cos(\varphi_+)\sin(\varphi_-) & \sin(\varphi_+)\cos(\varphi_-) & \cos(\varphi_+)\cos(\varphi_-) \end{pmatrix}, \tag{B11}$$

which can be written more compactly as in Eq. (5) in the main text.

## APPENDIX C: COVARIANCE MATRICES IN THE PRESENCE OF LOSSES

A photon loss associated with a given mode $S$, described by the density operator $\hat{\rho}$ and the corresponding covariance matrix $\sigma$, can be modeled by making use of a fictitious beam splitter with transmittivity $\eta$. The external environment on the second channel of the beam splitter is assumed to be in the vacuum state, while the output state in the first "physical" channel is obtained by tracing on the second one. The quantum channel $\Phi_\eta$ obtained in this way is called the attenuator channel,

$$\Phi_\eta(\hat{\rho}) = \mathrm{Tr}(\hat{U}_{\mathrm{BS}}\,\hat{\rho} \otimes |0\rangle_E\langle 0|\hat{U}_{\mathrm{BS}}^\dagger)_E, \tag{C1}$$

where the subscript $E$ denotes the environment and $\hat{U}_{\rm BS}$ is the unitary operator describing a beam splitter. As shown in Appendix B, the beam splitter is described by the unitary matrix

$$\mathcal{U}_{\rm BS}(\alpha) = \begin{pmatrix} \cos(\alpha) & -i\sin(\alpha) \\ -i\sin(\alpha) & \cos(\alpha) \end{pmatrix} = e^{i\alpha\sigma_x}, \tag{C2}$$

where $\eta = \cos(\alpha)^2$, corresponding [by using Eq. (B7)] to the symplectic rotation in phase space

$$O_{\rm BS}(\alpha) = \begin{pmatrix} \cos(\alpha)\,\mathbb{1}_2 & i\sin(\alpha)\,\sigma_y \\ i\sin(\alpha)\,\sigma_y & \cos(\alpha)\,\mathbb{1}_2 \end{pmatrix}. \tag{C3}$$

Thus, the covariance matrix

$$\sigma_{\rm SE} = \begin{pmatrix} \sigma & 0 \\ 0 & \frac{1}{2}\mathbb{1}_2 \end{pmatrix}, \tag{C4}$$

describing the system $S$, with covariance matrix $\sigma$, and the environment $E$ in the vacuum state, is transformed by the interaction with the beam splitter as

$$O_{\rm BS}(\alpha)\,\sigma_{\rm SE}\,O_{\rm BS}(\alpha)^T = \begin{pmatrix} \cos(\alpha)^2\,\sigma + \frac{1}{2}\sin(\alpha)^2\,\mathbb{1}_2 & i\sin(\alpha)\cos(\alpha)\big(\sigma - \frac{1}{2}\mathbb{1}_2\big)\sigma_y \\ -i\sin(\alpha)\cos(\alpha)\,\sigma_y\big(\sigma - \frac{1}{2}\mathbb{1}_2\big) & \frac{1}{2}\cos(\alpha)^2\,\mathbb{1}_2 + \cos(\alpha)^2\,\sigma_y\sigma\sigma_y. \end{pmatrix}. \tag{C5}$$

Therefore, a photon loss, described by the quantum channel in Eq. (C1), simply maps the (physical) covariance matrix into the covariance matrix of a convex combination of the signal with vacuum fluctuations,

$$\sigma \longmapsto \cos(\alpha)^2\,\sigma + \frac{1}{2}\sin(\alpha)^2\,\mathbb{1}_2 = \eta\,\sigma + \frac{1-\eta}{2}\mathbb{1}_2. \tag{C6}$$

The transformation above easily generalizes to an $M$-mode Gaussian state going through $M$ lossy lines with equal loss $\Phi_\eta^{\otimes M}$ as

$$\sigma \longmapsto \eta\,\sigma + \frac{1-\eta}{2}\mathbb{1}_{2M}. \tag{C7}$$

## APPENDIX D: DETECTION PROBABILITIES IN THE MACH-ZEHNDER INTERFEROMETER

The detection probability of our measurement in the presence of ideal detectors is given by

$$P = {\rm Tr}[\hat{S}_1(z_{\rm out})|00\rangle\langle 00|\hat{S}_1^\dagger(z_{\rm out})\hat{\rho}_{\rm MZ}] = (2\pi)^2 \int W_{\sigma_{\rm out}}(\boldsymbol{\xi})\,W_{\sigma_{\rm MZ}}(\boldsymbol{\xi})\,d^4\xi, \tag{D1}$$

with $\sigma_{\rm out}$ given in Eq. (8),

$$\sigma_{\rm MZ} = O_{\rm MZ}\sigma_{\rm in}O_{\rm MZ}^T, \tag{D2}$$

and $\sigma_{\rm in}$ given in Eq. (2). Thus, $P$ can also be expressed as

$$P = {\rm Tr}[|00\rangle\langle 00|\hat{S}_1^\dagger(z_{\rm out})\hat{\rho}_{\rm MZ}\hat{S}_1(z_{\rm out})] = (2\pi)^2 \int W_{\sigma_{\rm vac}}(\boldsymbol{\xi})\,W_{S_1(z_{\rm out})^{-1}\sigma_{\rm MZ}S_1(z_{\rm out})^{-1}}(\boldsymbol{\xi})\,d^4\xi, \tag{D3}$$

where $\sigma_{\rm vac} = \frac{1}{2}\mathbb{1}_4$ is the covariance matrix of the two-mode vacuum state and

$$S_1(z) = \begin{pmatrix} S(z) & 0 \\ 0 & \mathbb{1}_2 \end{pmatrix}, \tag{D4}$$

with $S(z)$ defined in Eq. (3),

$$S(z) = S(re^{i\theta}) = e^{i\theta\sigma_y}\begin{pmatrix} e^r & 0 \\ 0 & e^{-r} \end{pmatrix}e^{-i\theta\sigma_y}. \tag{D5}$$

A Gaussian integration of (D3) gives

$$P = \frac{1}{\sqrt{\det\left[\frac{1}{2}\mathbb{1}_4 + S_1(z_{\rm out})^{-1}\sigma_{\rm MZ}S_1(z_{\rm out})^{-1}\right]}}. \tag{D6}$$

If we introduce detectors with loss parameter $\eta$, modeled by attenuator channels right before them, the probability (D1) becomes

$$P = {\rm Tr}[|00\rangle\langle 00|\Phi_\eta \otimes \Phi_\eta(\hat{S}_1^\dagger(z_{\rm out})\hat{\rho}_{\rm MZ}\hat{S}_1(z_{\rm out}))], \tag{D7}$$

where $\Phi_\eta$ is the attenuator channel defined in Eq. (C1). Thus, applying the transformation (C7) to the second term in the determinant of Eq. (D6), we obtain

$$\begin{aligned} P &= \frac{1}{\sqrt{\det\left[\frac{1}{2}\mathbb{1}_4 + \eta S_1(z_{\rm out})^{-1}\sigma_{\rm MZ}S_1(z_{\rm out})^{-1} + \frac{1-\eta}{2}\mathbb{1}_4\right]}} \\ &= \det\left(\frac{2-\eta}{2}\mathbb{1}_4 + \eta S_1(z_{\rm out})^{-1}\sigma_{\rm MZ}S_1(z_{\rm out})^{-1}\right)^{-\frac{1}{2}} \\ &= \det[S_1(z_{\rm out})]^{-\frac{1}{2}}\det\left(\frac{2-\eta}{2}S_1(z_{\rm out})^2 + \eta\,\sigma_{\rm MZ}\right)^{-\frac{1}{2}}\det[S_1(z_{\rm out})]^{-\frac{1}{2}} \\ &= \det[(2-\eta)\,\sigma_{\rm out} + \eta\,\sigma_{\rm MZ}]^{-1/2}, \end{aligned} \tag{D8}$$

where in the last equality we used $\det[S_1(z_{\rm out})] = \det[S(z_{\rm out})] = 1$ and $\frac{1}{2}S_1(z_{\rm out})^2 = \sigma_{\rm out}$.

By making use of expressions (4), (5), and (2) for $\sigma_{\rm MZ}$, $O_{\rm MZ}$, and $\sigma_{\rm in}$, after some tedious but simple algebra we finally get

$$P(\beta,\varphi_-) = (1+\tilde{\eta}\{2N + [2\cos(\varphi_-)^2 + \tilde{\eta}\sin(\varphi_-)^4]N^2 - 2\cos(\varphi_-)^2\cos(2\beta)N(1+N)\})^{-1/2}, \tag{D9}$$

as claimed in the main text.

The counterpart of the previous probability when the antisqueezing is performed on the second channel can be calculated with the analogous equation

$$\begin{aligned} P'(\beta,\varphi_-) &= \mathrm{Tr}[|00\rangle\langle 00|\Phi_\eta\otimes\Phi_\eta(\hat{S}_2^\dagger(z_{\rm out})\hat{\rho}_{\rm MZ}\hat{S}_2(z_{\rm out}))] \\ &= (1+\tilde{\eta}\{2N + [2\sin(\varphi_-)^2 + \tilde{\eta}\cos(\varphi_-)^4]N^2 - 2\sin(\varphi_-)^2\cos(2\beta)N(1+N)\})^{-1/2}, \end{aligned} \tag{D10}$$

where $\hat{S}_2(z) = e^{\frac{1}{2}(z\hat{a}_2^{\dagger 2} - z^*\hat{a}_2^2)}$. This gives Eq. (25) in the main text.

Finally, the detection probability under internal losses, i.e., when the attenuator channel is applied before the antisqueezing operation, is given by

$$P''(\beta,\varphi_-) = \mathrm{Tr}[|00\rangle\langle 00|\hat{S}_1^\dagger(z_{\rm out})\Phi_\eta\otimes\Phi_\eta\big(\hat{\rho}_{\rm MZ}\big)\hat{S}_1(z_{\rm out})]. \tag{D11}$$

Thus, using the transformation (C7) on $\sigma_{\rm MZ}$ in the determinant of Eq. (D6), we obtain

$$\begin{aligned} P''(\beta,\varphi_-) &= \frac{1}{\sqrt{\det\left[\frac{1}{2}\mathbb{1}_4 + S_1(z_{\rm out})^{-1}\big(\eta\sigma_{\rm MZ} + \frac{1-\eta}{2}\mathbb{1}_4\big)S_1(z_{\rm out})^{-1}\right]}} \\ &= \det\left[S_1(z_{\rm out})^{-1}\left(\frac{1}{2}S_1^2(z_{\rm out}) + \eta\,\sigma_{\rm MZ} + \frac{1-\eta}{2}\,\mathbb{I}_4\right)S_1(z_{\rm out})^{-1}\right]^{-1/2} \\ &= \det[S_1(z_{\rm out})]^{-1/2}\det\left(\eta\,\sigma_{\rm MZ} + \frac{1-\eta}{2}\,\mathbb{I}_4 + \frac{1}{2}S_1^2(z_{\rm out})\right)^{-1/2}\det[S_1(z_{\rm out})]^{-1/2} \\ &= \det\left(\eta\,\sigma_{\rm MZ} + \frac{1-\eta}{2}\,\mathbb{I}_4 + \sigma_{\rm out}\right), \end{aligned} \tag{D12}$$

where in the last equality we used $\det[S_1(z_{\rm out})] = \det[S(z_{\rm out})] = 1$ and $\frac{1}{2}S_1(z_{\rm out})^2 = \sigma_{\rm out}$. This is Eq. (26) in the main text.

## APPENDIX E: LOCALIZATION OF THE PROBABILITY PEAKS

The diameters of a given level curve of the probability $P$ in Eq. (D9) are found simply by intersecting it with each of the coordinate axes. Let $P_0 \in (0,1)$ be fixed; then the intersections with the $\beta$ axis are found from the equation

$$P(\beta_*,0) = [1+4\tilde{\eta}N(1+N)\sin(\beta_*)^2]^{-1/2} = P_0, \tag{E1}$$

which immediately yields

$$\sin(\beta_*)^2 = \frac{1-P_0^2}{4\tilde{\eta}N(1+N)P_0^2}, \tag{E2}$$

as claimed in Eq. (16) in the main text. Analogously, the intersections with the $\varphi_-$ axis are the solutions to

$$P(0,\varphi_*) = [1+\tilde{\eta}^2N^2\sin(\varphi_*)^4 + 2\tilde{\eta}N\sin(\varphi_*)^2]^{-1/2} = P_0. \tag{E3}$$

This is a second-degree equation for $\sin(\varphi_*)^2$,

$$\tilde{\eta}^2N^2\sin(\varphi_*)^4 + 2\tilde{\eta}N\sin(\varphi_*)^2 - \frac{1-P_0^2}{P_0^2} = 0, \tag{E4}$$

which admits the solution

$$\sin(\varphi_*)^2 = \frac{\sqrt{P_0^2 + \tilde{\eta}\big(1-P_0^2\big)} - P_0}{\tilde{\eta}NP_0}, \tag{E5}$$

i.e., Eq. (17) in the main text.

[1] C. M. Caves, Quantum-mechanical noise in an interferometer, Phys. Rev. D **23**, 1693 (1981).

[2] B. Yurke, S. L. McCall, and J. R. Klauder, SU(2) and SU(1, 1) interferometers, Phys. Rev. A **33**, 4033 (1986).

[3] M. J. Holland and K. Burnett, Interferometric Detection of Optical Phase Shifts at the Heisenberg Limit, Phys. Rev. Lett. **71**, 1355 (1993).

[4] V. Giovannetti, S. Lloyd, and L. Maccone, Quantum-enhanced measurements: Beating the standard quantum limit, Science **306**, 1330 (2004).

[5] V. Giovannetti, S. Lloyd, and L. Maccone, Quantum Metrology, Phys. Rev. Lett. **96**, 010401 (2006).

[6] V. Giovannetti, S. Lloyd, and L. Maccone, Advances in quantum metrology, Nat. Photonics **5**, 222 (2011).

[7] L. Pezzè and A. Smerzi, Quantum theory of phase estimation, in *Proceedings of the International School of Physics "Enrico Fermi"* (IOP Press, Varenna, Italy, 2014), p. 691.

[8] R. Demkowicz-Dobrazánski, M. Jarzyna, and J. Kołodyński, Quantum limits in optical interferometry, Prog. Opt. **60**, 345 (2015).

[9] S. Steinert, F. Dolde, P. Neumann, A. Aird, B. Naydenov, G. Balasubramanian, F. Jelezko, and J. Wrachtrup, High sensitivity magnetic imaging using an array of spins in diamond, Rev. Sci. Instrum. **81**, 043705 (2010).

[10] L. T. Hall, G. C. G. Beart, E. A. Thomas, D. A. Simpson, L. P. McGuinness, J. H. Cole, J. H. Manton, R. E. Scholten, F. Jelezko, J. Wrachtrup, S. Petrou, and L. C. L. Hollenberg, High spatial and temporal resolution wide-field imaging of neuron activity using quantum NV-diamond, Sci. Rep. **2**, 401 (2012).

[11] L. M. Pham, D. Le Sage, P. L. Stanwix, T. K. Yeung, D. Glenn, A. Trifonov, P. Cappellaro, P. R. Hemmer, M. D. Lukin, H. Park, A. Yacoby, and R. L. Walsworth, Magnetic field imaging with nitrogen-vacancy ensembles, New J. Phys. **13**, 045021 (2011).

[12] M. Seo, A. Adam, J. Kang, J. Lee, S. Jeoung, Q. H. Park, P. Planken, and D. Kim, Fourier-transform terahertz near-field imaging of one-dimensional slit arrays: Mapping of electric-field-, magnetic-field-, and Poynting vectors, Opt. Express **15**, 11781 (2007).

[13] T. Baumgratz and A. Datta, Quantum Enhanced Estimation of a Multidimensional Field, Phys. Rev. Lett. **116**, 030801 (2016).

[14] P. C. Humphreys, M. Barbieri, A. Datta, and I. A. Walmsley, Quantum Enhanced Multiple Phase Estimation, Phys. Rev. Lett. **111**, 070403 (2013).

[15] J. Liu, X.-M. Lu, Z. Sun, and X. Wang, Quantum multiparameter metrology with generalized entangled coherent state, J. Phys. A: Math. Theor. **49**, 115302 (2016).

[16] J.-D. Yue, Y.-R. Zhang, and H. Fan, Quantum-enhanced metrology for multiple phase estimation with noise, Sci. Rep. **4**, 5933 (2014).

[17] P. A. Knott, T. J. Proctor, A. J. Hayes, J. F. Ralph, P. Kok, and J. A. Dunningham, Local versus global strategies in multiparameter estimation, Phys. Rev. A **94**, 062312 (2016).

[18] C. N. Gagatsos, D. Branford, and A. Datta, Gaussian systems for quantum-enhanced multiple phase estimation, Phys. Rev. A **94**, 042342 (2016).

[19] M. A. Ciampini, N. Spagnolo, C. Vitelli, L. Pezzé, A. Smerzi, and F. Sciarrino, Quantum-enhanced multiparameter estimation in multiarm interferometers, Sci. Rep. **6**, 28881 (2016).

[20] Z. Eldredge, M. Foss-Feig, J. A. Gross, S. L. Rolston, and A. V. Gorshkov, Optimal and secure measurement protocols for quantum sensor networks, Phys. Rev. A **97**, 042337 (2018).

[21] K. Arai, C. Belthangady, H. Zhang, N. Bar-Gill, S. J. DeVience, P. Cappellaro, A. Yacoby, and R. L. Walsworth, Fourier magnetic imaging with nanoscale resolution and compressed sensing speed-up using electronic spins in diamond, Nat. Nanotechnol. **10**, 859 (2015).

[22] A. Lazariev and G. Balasubramanian, A nitrogen-vacancy spin based molecular structure microscope using multiplexed projection reconstruction, Sci. Rep. **5**, 14130 (2015).

[23] P. Komar, E. M. Kessler, M. Bishof, L. Jiang, A. S. Sørensen, J. Ye, and M. D. Lukin, A quantum network of clocks, Nat. Phys. **10**, 582 (2014).

[24] T. J. Proctor, P. A. Knott, and J. A. Dunningham, Multiparameter Estimation in Networked Quantum Sensors, Phys. Rev. Lett. **120**, 080501 (2018).

[25] S. Boixo, S. T. Flammia, C. M. Caves, and J. M. Geremia, Generalized Limits for Single-Parameter Quantum Estimation, Phys. Rev. Lett. **98**, 090401 (2007).

[26] M. D. Lang and C. M. Caves, Optimal Quantum-Enhanced Interferometry Using a Laser Power Source, Phys. Rev. Lett. **111**, 173601 (2013).

[27] Q. Zhuang, Z. Zhang, and J. H. Shapiro, Distributed quantum sensing using continuous-variable multipartite entanglement, Phys. Rev. A **97**, 032329 (2018).

[28] X. Guo, C. R. Breum, J. Borregaard, S. Izumi, M. V. Larsen, T. Gehring, M. Christandl, J. S. Neergaard-Nielsen, and U. L. Andersen, Distributed quantum sensing in a continuous variable entangled network, Nat. Phys. **16**, 281 (2020).

[29] G. Gramegna, D. Triggiani, P. Facchi, F. A. Narducci, and V. Tamma, Heisenberg scaling precision in multi-mode distributed quantum metrology, New J. Phys. **23**, 053002 (2021).

[30] G. Gramegna, D. Triggiani, P. Facchi, F. A. Narducci, and V. Tamma, Typicality of Heisenberg scaling precision in multimode quantum metrology, Phys. Rev. Res. **3**, 013152 (2021).

[31] M. Takeoka, K. P. Seshadreesan, C. You, S. Izumi, and J. P. Dowling, Fundamental precision limit of a Mach-Zehnder interferometric sensor when one of the inputs is the vacuum, Phys. Rev. A **96**, 052118 (2017).

[32] D. Triggiani, P. Facchi, and V. Tamma, Heisenberg scaling precision in the estimation of functions of parameters in linear optical networks, Phys. Rev. A **104**, 062603 (2021).

[33] Y. Xia, W. Li, W. Clark, D. Hart, Q. Zhuang, and Z. Zhang, Demonstration of a Reconfigurable Entangled Radio-Frequency Photonic Sensor Network, Phys. Rev. Lett. **124**, 150502 (2020).

[34] L.-Z. Liu, Y.-Z. Zhang, Z.-D. Li, R. Zhang, X.-F. Yin, Y.-Y. Fei, L. Li, N.-L. Liu, F. Xu, Y.-A. Chen, and J.-W. Pan, Distributed quantum phase estimation with entangled photons, Nat. Photonics **15**, 137 (2021).

[35] Y. Xia, W. Li, Q. Zhuang, and Z. Zhang, Quantum-Enhanced Data Classification with a Variational Entangled Sensor Network, Phys. Rev. X **11**, 021047 (2021).

[36] S.-R. Zhao, Y.-Z. Zhang, W.-Z. Liu, J.-Y. Guan, W. Zhang, C.-L. Li, B. Bai, M.-H. Li, Y. Liu, L. You, J. Zhang, J. Fan, F. Xu, Q. Zhang, and J.-W. Pan, Field Demonstration of Distributed Quantum Sensing without Post-selection, Phys. Rev. X **11**, 031009 (2021).

[37] D. Gatto, P. Facchi, F. A. Narducci, and V. Tamma, Distributed quantum metrology with a single squeezed-vacuum source, Phys. Rev. Res. **1**, 032024(R) (2019).

[38] A. M. Marino, N. V. Corzo Trejo, and P. D. Lett, Effect of losses on the performance of an SU(1, 1) interferometer, Phys. Rev. A **86**, 023844 (2012).

[39] C. Oh, C. Lee, S. Hyung Lie, and H. Jeong, Optimal distributed quantum sensing using Gaussian states, Phys. Rev. Res. **2**, 023030 (2020).

[40] W. P. Schleich, *Quantum Optics in Phase Space* (Wiley-VCH, Berlin, 2001).

[41] D. Gatto, P. Facchi, and V. Tamma, Phase space Heisenberg-limited estimation of the average phase shift in a Mach-Zehnder interferometer, Int. J. Quantum Inf. **18**, 1941019 (2020).

[42] P. Stoica and T. L. Marzetta, Parameter estimation problems with singular information matrices, IEEE Trans. Signal Process. **49**, 87 (2001).

[43] P. Stoica and T. Söderström, On non-singular information matrices and local identifiability, Int. J. Control **36**, 323 (1982).

[44] Y.-H. Li and P.-C. Yeh, An interpretation of the Moore-Penrose generalized inverse of a singular Fisher information matrix, IEEE Trans. Signal Process. **60**, 5532 (2012).

[45] T. J. Rothenberg, Identification in parametric models, Econometrica **39**, 577 (1971).

[46] A. De Pasquale, D. Rossini, P. Facchi, and V. Giovannetti, Quantum parameter estimation affected by unitary disturbance, Phys. Rev. A **88**, 052117 (2013).